Laser-assisted selective and localized surface transformation of titanium to anatase, rutile, and mixed phase nanostructures

Cite as: J. Laser Appl. **33**, 012014 (2021); https://doi.org/10.2351/7.0000316
Submitted: 30 November 2020 . Accepted: 30 November 2020 . Published Online: 22 December 2020

Parvin Fathi-Hafshejani, Haden Johnson, Zabihollah Ahmadi, Michael Roach, Nima Shamsaei, and Masoud Mahjouri-Samani

Journal of Laser Applications ARTICLE scitation.org/journal/jla

Laser-assisted selective and localized surface transformation of titanium to anatase, rutile, and mixed phase nanostructures

Cite as: J. Laser Appl. 33, 012014 (2021); doi: 10.2351/7.0000316
Submitted: 30 November 2020 · Accepted: 30 November 2020 ·
Published Online: 22 December 2020

Parvin Fathi-Hafshejani,[1] Haden Johnson,[2] Zabihollah Ahmadi,[1] Michael Roach,[2] Nima Shamsaei,[3,4] and Masoud Mahjouri-Samani[1,4,a)]

AFFILIATIONS

[1]Department of Electrical and Computer Engineering, Auburn University, Auburn, Alabama 36849
[2]Department of Biomedical Materials Science, University of Mississippi Medical Center, Jackson, Mississippi 39216
[3]Department of Mechanical Engineering, Auburn University, Auburn, Alabama 36849
[4]National Center for Additive Manufacturing Excellence (NCAME), Auburn University, Auburn, Alabama 36849

Note: Paper published as part of the special topic on Proceedings of the International Congress of Applications of Lasers & Electro-Optics 2020.

[a)]**Author to whom correspondence should be addressed; electronic mail:** mahjouri@auburn.edu

ABSTRACT

Titanium dioxide (TiO_2) has been a key material in a wide range of applications such as catalysis, energy harvesting, and antibacterial surfaces. Typically, different TiO_2 phases are first synthesized and then coated onto the test parts. Here, the authors demonstrate a direct method for the formation of TiO_2 nanostructures and patterns with rutile, anatase, and mixed phases by a controlled laser-assisted surface modification approach on additive manufacturing titanium parts. A tunable nanosecond fiber laser coupled to a galvo scanner was employed to regulate the laser material for a controlled and localized transformation process in an oxygen environment. The influence of processing conditions such as scanning speed, laser power, laser pulse duration, frequency, and gas flow rate on the selective formation of rutile, anatase, and mixed phases was studied. The structural evolutions and morphology have been investigated using different characterization techniques, including scanning electron microscopy and Raman spectroscopy methods. The main advantage of this laser-assisted process is its ability to create selective TiO_2 phases on complex titanium parts such as implants.

Key words: additive manufacturing, laser surface modification, titanium dioxide, laser processing, nanostructures

I. INTRODUCTION

Titanium dioxide (TiO_2) has been widely used in many energy and biological applications due to its excellent photocatalytic, antibacterial, and energy storage properties. The performance of TiO_2 is affected significantly by the modification of chemical compositions, physical structures, and phases.[1–6] The most common phases of TiO_2 include rutile, anatase, and brookite.[7] Recent trends in the three-dimensional micro/nanostructured TiO_2 with improved performance have led to an explosion of studies regarding its applications due to its unique properties such as large surface area, superior light-harvesting capacity, and antibacterial characteristics.[8–13] For instance, TiO_2 has attracted much attention due to its excellent photocatalytic performance in water splitting when illuminated by ultraviolet light.[6,14,15] An exciting example is the use of TiO_2 for the formation of antibacterial surfaces, especially on titanium parts such as bio implant or titanium-based biomedical devices.[16–18]

Since the properties of TiO_2 depend on its phase and morphology, it is important to have precise control over their synthesis.[19] Various techniques have been used to synthesize TiO_2 structures and films on titanium parts, including thermal spray with different powder particles, chemical vapor deposition,

electrochemical anodization, sputtering technique, and pulse laser deposition.[1,2,8,13,20,21] Although these procedures can create TiO_2 coatings with distinctive phases, they are not suitable for localized, patterned, and selective phase depositions, particularly on the parts with complex geometries. Subsequently, the advancement of simple strategies for the manufacture of substrate-grown TiO_2 with the designable morphology and structures is exceedingly interesting.

Here, we introduce a laser-based technique for the fabrication of TiO_2-based nanomaterials on titanium parts. In this procedure, we use the laser to create localized heat on the surface of titanium parts and induce chemical reaction under the oxygen environment to form a thin layer of TiO_2 with control over its phase, morphology, and location. The phase and morphology of the synthesized TiO_2 coatings can be readily controlled by tuning the laser processing conditions such as scan speed, laser power, frequency, and pulse-width.

II. EXPERIMENT

Lasers provide the ability to apply precise amounts of energy onto a confined location in order to induce desired physical modification or chemical reaction that can be accurately tuned by the laser control parameters. For opaque parts, this energy is mainly retained close to the surface, enabling the formation of multiscale crystal structures on the surface without modifying the bulk. Irradiation of a target material with nanosecond laser pulses leads to the formation of a high-temperature melt pool as well as a confined plasma at atmospheric pressures. The presence of reactive atoms such as oxygen will, therefore, initiate chemical reactions and modification of the laser-treated titanium parts and hence leading to the formation of TiO_2 structures. The phase and morphology of this TiO_2 layer are then controlled by adjusting the laser process parameters.

A. Materials

Two types of titanium material were used, including pure titanium sheet (purity 99.99%) and additively manufactured disc (10 mm in diameter). Additive manufacturing samples were made by a laser beam powder bed fusion (LB-PBF) process using the EOS M290 machine, with the manufacturer's parameters of 1200 mm/s scanning speed, 0.14 mm hatching space, 280 W laser power, and 30 mm layer thickness using Ti-6Al-4V Powder: LPW-Ti64GD23-AAFD.

B. TiO_2 formation process

Figure 1 illustrates the schematic of the laser surface modification process. First, the titanium samples were washed with acetone and methanol. Samples were then placed into a custom-built environmental chamber for laser processing. The laser surface modification experiments were done in an oxygen environment at various flow rates (6–60 slm) and at room temperature. First, the possible air contaminants in the chamber were removed by flushing with oxygen gas for a few minutes. TiO_2 phases were then controllably synthesized by a 130 W tunable nanosecond fiber laser (1064 nm wavelength), capable of emitting nanosecond pulses (5–2000 ns in 63 pulse-width) with pulse energy ranging from 0.04 to 1.57 mJ, a repetition rate of 1 Hz to 4160 kHz. According to the manufacturer datasheets, the laser beam has a Gaussian shape that is randomly polarized. The laser beam was coupled into a galvo scanner and focused onto the samples through an f-theta lens with 103 mm focal length producing a spot size of about 18 μm. The laser spot size was calculated using $d = (k \cdot M^2 \cdot \lambda \cdot f)/D$, where λ is the wavelength (1064 nm), f is the focal length (l03 mm for our f-theta lens), M^2 is the beam quality (1.3), k is the correction factor (1.27), and D is the entrance beam diameter (~1 cm).

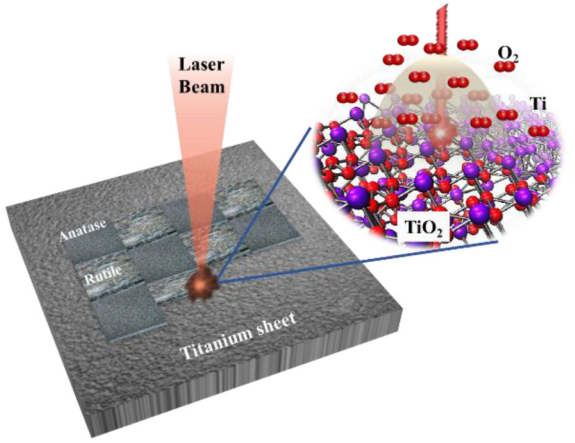

FIG. 1. Schematic presentation showing the scanning titanium surface where titanium and oxygen react to form anatase or rutile TiO_2 nanostructures depending on the process parameters.

A laser software (Laser Studio Professional) was utilized to control the process parameters (e.g., pulse-width, power, scan speed, number of pulses, overlaps, and repetition rate) and design various patterns of interest.

C. Raman spectroscopy

The Raman spectra were acquired from the synthesized TiO_2 parts using a custom-built Raman spectroscopy system with a 532 nm laser excitation source, 1200 l mm^{-1} grating, and 10/50× objective lenses.

D. Morphology and structure analysis

A scanning electron microscope (SEM; Zeiss Supra 40, Jena, Germany) with an accelerating voltage of 3 kV was used to monitor the surface morphology of the laser synthesized oxides.

III. RESULT AND DISCUSSION

In order to understand how the laser parameter can influence the interaction between titanium and oxygen, the impact of laser energy on the titanium surface was studied. The amount of applied energy in this work directly depends on the combination of laser power, speed, and pulse-width. Therefore, to find the behavior of the reaction as well as the resulting phases of nanoparticles, systematic experiments were performed. Various process parameters

including six different scan speeds (100, 200, 500, 1000, 2000, and 5000 mm/s), laser power ranging from 13 to 71 W, and six pulse-widths (261, 108, 10, 508, 1020, and 2020 ns) were tested. Figure 2 shows a heatmap of the rutile, mixed rutile/anatase, anatase, and unchanged zones as a function of laser scan speed and laser power using the laser pulse-width of 508 nm and 108 kHz repetition rate on pure titanium (purity 99.99%) sheets. The scan speed determines the pulse overlap (pitch), and the line hatch has 40% overlap. The energy for each pulse altered from 0.125 mJ for 13.5 W to 0.687 mJ for 74 W power with the fluence of 47 and 270 J/cm^2, respectively.

In general, rutile formation was more favorable for slower scan speeds and higher laser powers due to the generation of more heat, while faster scan speed and lower laser power change the kinetics to the anatase growth zone by generating less heat. It was noticed that the process window for the formation of rutile (red zone) was much larger than the anatase and mixed-phase process windows. The anatase formation was quite sensitive to process variation (i.e., induced heat), as shown by its small crystallization area (green), and could easily convert into mixed or rutile phases. This required very careful process parameters control to ensure the formation of high-quality anatase coatings. The zone between process parameters of anatase and rutile produced mixed anatase/rutile phases (orange). Furthermore, the pulse-width study confirmed that the longer pulse durations generate more heat than that of small pulses duration, which in turn requires more speed or less power to balance for the needed transformation energies in each region.

In addition, we found that the distance between the scanning lines (hatch) and overlap between pulses (pitch) had a considerable impact on the resulting heat, chemical reaction, phase evolution, and morphology of the final structures. Another parameter that played an important role was the laser repetition rate by which we could tune the pulse off-time during each cycle and hence adjust the cooling time for each pulse. For example, at lower frequencies

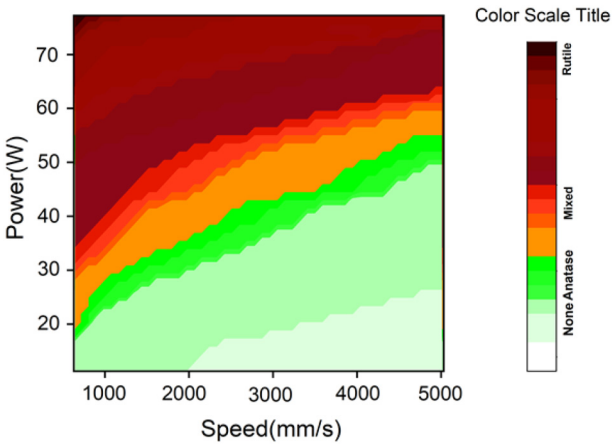

FIG. 2. A comprehensive processing map of the material's response to different laser speed and power. Red, green, and orange zones show the rutile, anatase, and mixed-phase formation regions, respectively.

TABLE I. Laser parameters to synthesize different titanium phases.

TiO_2 phase	Rutile	Mixed	Anatase
Laser power (W)	62.5	67.5	12.5
Scan speed (mm/s)	200	400	400
Pulse-width (ns)	508	508	508
Pulse energy (mJ)	0.625	0.337	0.625
Pulse fluence (J/cm^2)	246	133	246
Gas flow rate (slm)	21.3	25.6	25.6
Pulse overlap (%)	90	50	0
Line hatch (%)	0	0	40
Frequency (kHz)	100	200	20

(e.g., 20 kHz), the time between each pulse called off-time increases, so it provides more delay time before the next pulse arrives. This hence gives TiO_2 crystals more time to cool down per pulse. This fast heat quenching of the reaction per pulse caused the formation of anatase nanoparticles, which were well-attached to the surface. In this step, the systematic experiments were designed to track the impact of off-time and overlapping pulses, which depends on the repetition rate (frequency). In this study, we kept scan speed and power constant and change pulse overlapping, hatch, frequency, and pulse-width. Experiments were done with three different overlaps (0%, 50%, and 90%), two hatches, which were 40% and 0% between lines under a number of different frequencies. We also tested these parameters for six different pulse-widths (261, 108, 10, 508, 1020, and 2020 ns). As anticipated, at higher frequencies (e.g., 100 kHz), the off-time between pulses decreased (~9.5 μs)

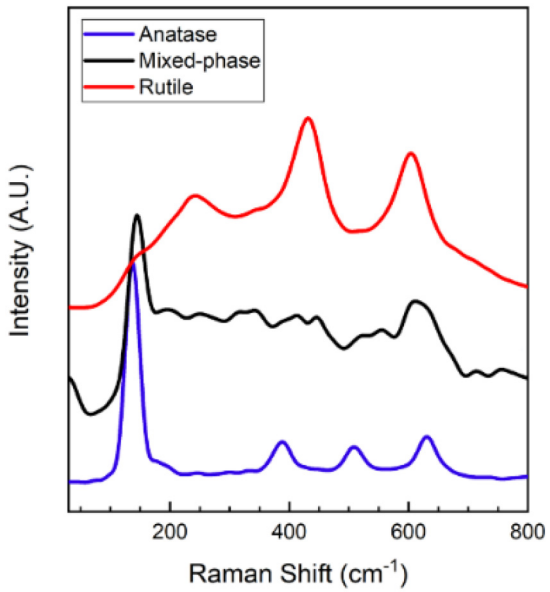

FIG. 3. Representative Raman spectra of the synthesized TiO_2 structures on additively manufactured samples showing the successful formation of rutile, anatase, and mixed-phase TiO_2 coatings.

that resulted in increasing the heat accumulation, and consequently, the formation of high-quality TiO_2 rutile structures. At lower frequencies (e.g., 20 kHz), the off-time between pulses increased (~49.5 μs) by five times more than the rutile formation case, which let the material cool down between the pulses, resulting in the formation of high-quality anatase structures. Similarly, having less overlap (e.g., 0%) between the scanned spots created anatase structures. On the other hand, more overlap (e.g., 90%) created rutile structures because of the more heating. As expected, when the crystal had enough time to cool, better anatase could be produced, which were bonded to the surface. This initial experiment led us to fine-tune and optimize the process parameters, as indicated in Table I.

To monitor the conversion process and detect the TiO_2 phases, Raman spectroscopy measurements were performed on the samples synthesized in each experiment. Figure 3 shows the Raman spectra attained from the rutile, anatase, and mixed phases, which is produced by the parameters in Table I. Rutile samples exhibited peaks at 241, 445, and 610 cm^{-1}, while anatase samples emitted clear Raman peaks at 145, 198, 399, 516, and 638 cm^{-1}. The mixed-phase samples have the mark of both rutile and anatase. These Raman results were comparable to the results described in the literature,[22] verifying the successful creation of various TiO_2 phases in this procedure.

Figure 4 exhibits the SEM images of rutile, mixed-phase, and anatase TiO_2 made on the surface of additively manufactured samples. The morphology of the rutile TiO_2 layers was larger, with big cracks showing the ceramic nature of the rutile structures, as shown in Fig. 4(a). As shown in Fig. 4(c), the size and morphology of the anatase specimens were micro/nanostructures with a porous morphology, while mixed-phase TiO_2 showed both cracks and porous structures, as shown in the figure. According to the cross-sectional SEM imaging of the laser-modified samples, the thickness of the rutile layer was in the order of 2 μm, whereas the thickness for mixed-phase and anatase became thinner with about ~0.4 and ~0.3 μm, respectively.

One of the most important benefits of this technique is its ability for the localized and selective synthesis of different phases, side-by-side patterns, and sizes without any requirement for complicated lithography, patterning, and deposition processes. To demonstrate this ability, we successfully synthesized designed patterns of rutile, anatase, and mixed-phase TiO_2 structures on the titanium parts. Figure 5(a) shows the optical images of rutile and anatase patterns side-by-side in the checkerboard.

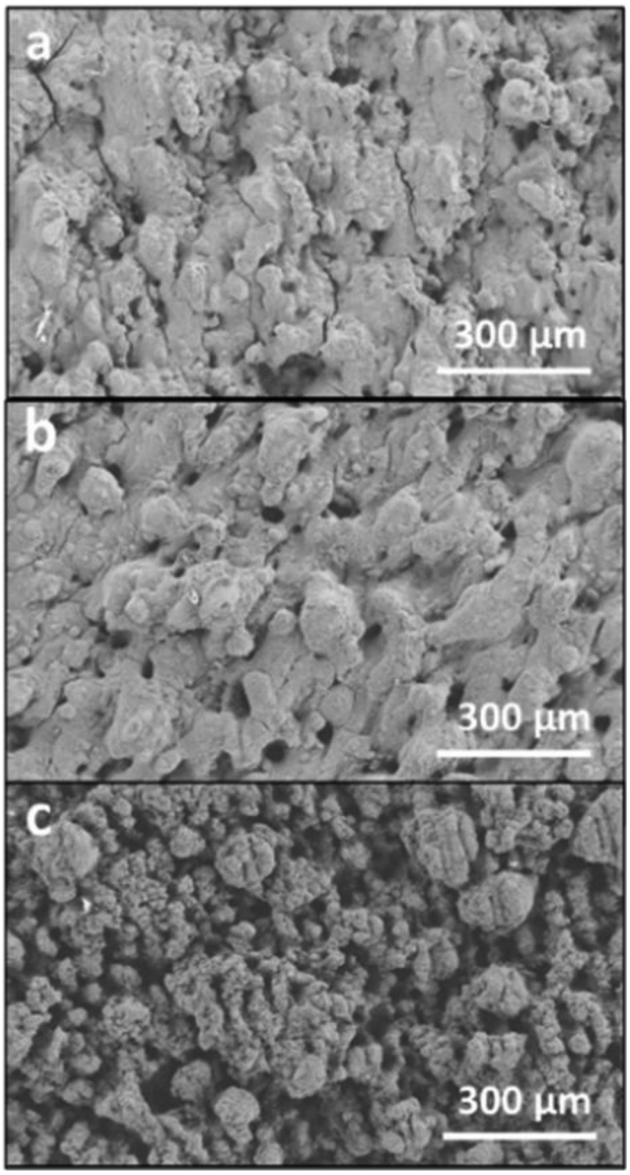

FIG. 4. SEM images showing the morphology of additively manufactured TiO_2 rutile (a), mixed-phase (b), and anatase (c) nanostructures.

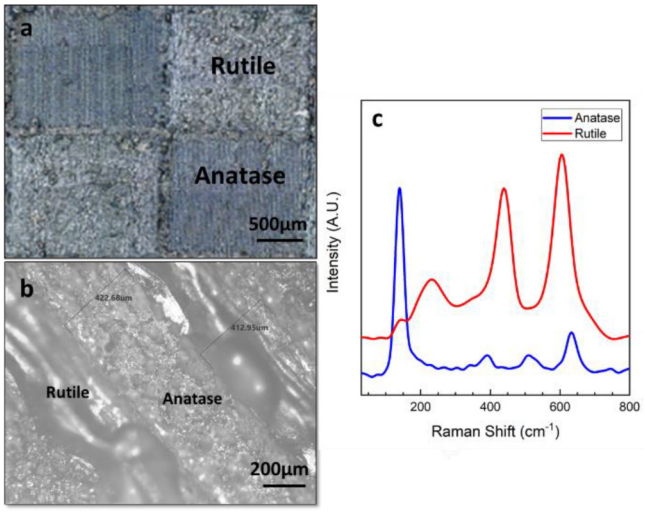

FIG. 5. Side-by-side formation of anatase and rutile TiO_2. Optical images show and checkers board (a), stripe patterns (b), and anatase and rutile TiO_2 Raman gain from checkers board pattern (c).

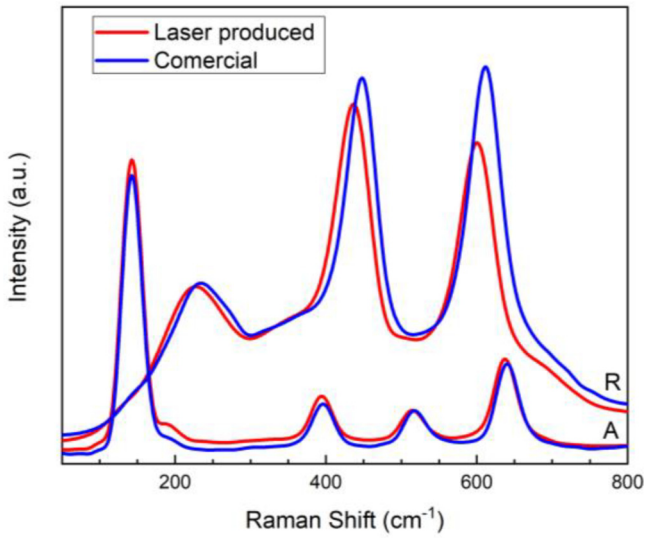

FIG. 6. TiO_2 quality comparison of the laser-generated (red curves) vs the commercially available (blue curves) anatase (A) and rutile (R) samples, both showing similar Raman signatures.

Additionally, in these experiments, we could synthesize anatase and rutile side by side in a stripe pattern with a good resolution. Resolution is defined by the laser spot size (18 μm in our case) plus the heat-affected zone. For example, considering the heat affected zone for each phase (i.e., less for anatase and more for rutile), the resolution is about 30 and 50 μm for anatase and rutile, respectively. This could be further improved by choosing F-theta lenses with smaller spot sizes. Figure 5(b) exhibits the optical images of various stripe patterns.

Finally, we compared the quality of the formed TiO_2 structures with that of commercially available high-quality powders, as shown in Fig. 6. Both anatase and rutile structures showed Raman vibration modes very similar to the commercial samples.

IV. CONCLUSION

In conclusion, we demonstrated a direct laser processing method for the fabrication of substrate-grown TiO_2 nanostructures with different phases and structures. We introduced the influence of laser powers, scan speed, and pulse-width, followed by controlling the overlap between the pulses to controllably produce high-quality anatase, rutile, and mixed-phase TiO_2 coating on the titanium parts. We also displayed the effect of off-time between pulses on the phase-selective transformation. In general, longer off-time resulted in the phase conversion toward anatase TiO_2, and shorter off-time resulted in the formation of the rutile phase. We showed that TiO_2 coating with different phases and structures could be formed side-by-side simply by adjusting the laser process parameter during the process in real time. This method allows for a clean, simple, and fast growth of TiO_2 coating on titanium surfaces, specifically the customized, additive manufacturing parts, with possible application in future customized bio-implant parts.

REFERENCES

[1]T. Zhao, Y. Zhao, and L. Jiang, "Nano-/microstructure improved photocatalytic activities of semiconductors," Philos. Trans. R. Soc. A Math. Phys. Eng. Sci. **371**, 20120303 (2013).
[2]R. Asahi, T. Morikawa, H. Irie, and T. Ohwaki, "Nitrogen-doped titanium dioxide as visible-light-sensitive photocatalyst: Designs, developments, and prospects," Chem. Rev. **114**, 9824–9852 (2014).
[3]A. Pearson, H. Zheng, K. Kalantar-Zadeh, S. K Bhargava, and V. Bansal, "Decoration of TiO_2 nanotubes with metal nanoparticles using polyoxometalate as a UV-switchable reducing agent for enhanced visible and solar light photocatalysis," Langmuir **28**, 14470–14475 (2012).
[4]D. A. Hanaor and C. C. Sorrell, "Review of the anatase to rutile phase transformation," J. Mater. Sci. **46**, 855–874 (2011).
[5]R. Vijayalakshmi and V. Rajendran, "Synthesis and characterization of nano-TiO_2 via different methods," Arch. Appl. Sci. Res. **4**, 1183–1190 (2012).
[6]A. Fujishima, T. N. Rao, and D. A. Tryk, "Titanium dioxide photocatalysis," J. Photochem. Photobiol. C Photochem. Rev. **1**, 1–21 (2000).
[7]P. Löbl, M. Huppertz, and D. Mergel, "Nucleation and growth in TiO_2 films prepared by sputtering and evaporation," Thin Solid Films **251**, 72–79 (1994).
[8]K. Nakata and A. Fujishima, "TiO_2 photocatalysis: Design and applications," J. Photochem. Photobiol. C Photochem. Rev. **13**, 169–189 (2012).
[9]B. L. Ellis, P. Knauth, and T. Djenizian, "Three-dimensional self-supported metal oxides for advanced energy storage," Adv. Mater. **26**, 3368–3397 (2014).
[10]D. Fattakhova-Rohlfing, A. Zaleska, and T. Bein, "Three-dimensional titanium dioxide nanomaterials," Chem. Rev. **114**, 9487–9558 (2014).
[11]I. S. Cho, Z. Chen, A. J. Forman, D. R. Kim, P. M. Rao, T. F. Jaramillo, and X. Zheng, "Branched TiO_2 nanorods for photoelectrochemical hydrogen production," Nano Lett. **11**, 4978–4984 (2011).
[12]J. M. Frechet, "Dendrimers and other dendritic macromolecules from building blocks to functional assemblies in nanoscience and nanotechnology," J. Polym. Sci. A Polym. Chem. **41**, 3713–3725 (2003).
[13]S.-J. Bao, C. Lei, M.-W. Xu, C.-J. Cai, and D.-Z. Jia, "Environment-friendly biomimetic synthesis of TiO_2 nanomaterials for photocatalytic application," Nanotechnology **23**, 205601 (2012).
[14]A. Fujishima and K. Honda, "Electrochemical photolysis of water at a semiconductor electrode," Nature **238**, 37–38 (1972).
[15]D. Tryk, A. Fujishima, and K. Honda, "Recent topics in photoelectrochemistry: Achievements and future prospects," Electrochim. Acta **45**, 2363–2376 (2000).
[16]G. M. Crane, S. L. Ishaug, and A. G. Mikos, "Bone tissue engineering," Nat. Med. **1**, 1322–1324 (1995).
[17]M. Jokinen, M. Pätsi, H. Rahiala, T. Peltola, M. Ritala, and J. B. Rosenholm, "Influence of sol and surface properties on in vitro bioactivity of sol-gel-derived TiO_2 and TiO_2-SiO_2 films deposited by dip-coating method," J. Biomed. Mater. Res. **42**, 295–302 (1998).
[18]X. Liu, P. K. Chu, and C. Ding, "Surface modification of titanium, titanium alloys, and related materials for biomedical applications," Mater. Sci. Eng. R Rep. **47**, 49–121 (2004).
[19]S. Jain, R. S. Williamson, and M. D. Roach, "Surface characterization, shear strength, and bioactivity of anodized titanium prepared in mixed-acid electrolytes," Surf. Coat. Technol. **325**, 594–603 (2017).
[20]T.-K. Ahn, D. H. Lee, T.-S. Kim, G. C. Jang, S. J. Choi, J. B. Oh, G. Ye, and S. Lee, "Modification of titanium implant and titanium dioxide for bone tissue engineering," in *Novel Biomaterials for Regenerative Medicine* (Springer, New York, 2018), pp. 355–368.
[21]S. Biswas and U. Becker, "Molecular modeling of cell adhesion peptides on hydroxyapatite and TiO_2 surfaces: Implication in biomedical implant devices," J. Biomater. Nanobiotechnol. **4**, 351–356 (2013).
[22]W. Su, J. Zhang, Z. Feng, T. Chen, P. Ying, and C. Li, "Surface phases of TiO_2 nanoparticles studied by UV Raman spectroscopy and FT-IR spectroscopy," J. Phys. Chem. C **112**, 7710–7716 (2008).